New Results for the Open Cluster Bica 6 and Its Associated Planetary Nebula Abell 8

D. G. TURNER,[1]

Department of Astronomy and Physics, Saint Mary's University, Halifax, NS B3H 3C3, Canada; turner@ap.smu.ca,

J. M. ROSVICK,[1]

Department of Physical Sciences, Thompson Rivers University, 900 McGill Road, Kamloops, BC V2C 0C8, Canada,

D. D. BALAM

Dominion Astrophysical Observatory, Herzberg Institute of Astrophysics, National Research Council of Canada,
5071 West Saanich Road, Victoria, BC V6A 3K7, Canada

A. A. HENDEN

American Association of Variable Star Observers, 49 Bay State Road, Cambridge, MA 02138

AND

D. J. MAJAESS,[2] AND D. J. LANE[2]

Department of Astronomy and Physics, Saint Mary's University, Halifax, NS B3H 3C3, Canada

ABSTRACT. The likely membership of the planetary nebula Abell 8 (PN G167.0–00.9) in the open cluster Bica 6 is confirmed by CCD spectra, $UBV(RI)_C$ photometry, and radial velocities for luminous cluster stars. The reddening, estimated distance, and radial velocity of the planetary nebula agree with parameters derived for Bica 6 of $E_{B-V}(\text{mean}) = 0.42$, $d = 1.60 \pm 0.11$ kpc, and $V_R = 57 \pm 1$ km s^{-1}, with a cluster age of 10^9 yr, a diagnostic blue hook, and a few blue stragglers, including a peculiar B1 Vnn star (HDE 277593) that may be a post-AGB star. The results identify Bica 6 as a potential calibrator of the planetary nebula distance scale. The central star of the planetary nebula has a reddening of $E_{B-V} = 0.49 \pm 0.02$, with a possible circumnebular excess, and an estimated luminosity of $M_V = +7.44 \pm 0.16$. It is also an optical double in 2MASS images, with a likely progenitor according to evolutionary considerations being a late B-type dwarf of ∼2.3 $M_\odot$.

1. INTRODUCTION

The progenitors of planetary nebulae (PNe) are generally considered to have once been main-sequence stars with masses of up to ∼8 $M_\odot$ (e.g., Weidemann 2000), yet a practical demonstration of such a link has so far been limited by the paucity of PNe associated with intermediate-age open clusters, where physically associated, lower-mass, main-sequence progenitors may exist. Searches for possible planetary nebula (PN) and open cluster associations have revealed a number of potential spatial coincidences, as noted by Ziznovsky (1975) and Lubos Kohoutek (see Majaess et al. 2007), but available data on possible matches in radial velocity, reddening, and distance of the PNe and cluster stars are, as yet, unconvincing (e.g., Kiss et al. 2008). The relatively short duration of the PN evolutionary phase and the rapid rate of dissolution of open clusters conspire to make true physical links relatively rare, if they exist at all (Majaess et al. 2007).

The distances to individual PNe are also difficult to establish, resulting in a variety of techniques applied to the problem (Kaler 1985; Lutz 1989). If the central star is bright enough for photometric or spectroscopic observation, the distance can often be established through trigonometric or spectroscopic parallax. Trigonometric parallaxes, for example, have been derived for several PNe through the US Naval Observatory program (Pier et al. 1993; Harris et al. 1997, 2007), from measurements by the *Hipparcos* satellite (see Acker et al. 1998) and, most recently, measurements with the *Hubble Space Telescope* (Benedict et al. 2009). Spectroscopic parallaxes produce mixed results (e.g., Acker et al. 1998), which may relate to the models used and the quality of spectra for faint stars. Nebular expansion parallaxes have also been applied (Terzian 1997), despite their observational limitations (Terzian 1997) and initial assumptions

---

[1] Visiting Astronomer, Dominion Astrophysical Observatory, Herzberg Institute of Astrophysics, National Research Council of Canada.

[2] Abbey Ridge Observatory, Stillwater Lake, NS, Canada

(Kaler 1985). Indirect methods also exist, the most basic being the Shklovsky distance method (Shklovsky 1956), which is tied to estimates for the surface brightness of the surrounding PN shell, thus being limited by the difficulties of recording the spectra of PNe. Improved versions of the technique (e.g., Zhang 1995; Phillips 2004) typically involve measurement of the radio continuum surface brightness temperature T_b. Finally, it is possible to infer distances to PNe by using the reddening inferred from a comparison of line strengths for emission features in their spectra in conjunction with maps of reddening versus distance for stars observed along the line of sight to the nebula (Lutz 1973; Acker 1978; Gathier et al. 1986; Pollacco & Ramsay 1992). The recent IPHAS Hα survey of the Galactic plane has generated extensive visible/infrared photometry for many stars in the fields of PNe, thereby permitting extension of the technique to a greater selection of PNe (Sale et al. 2009), as done by Giammanco et al. (2011).

As a result of many such studies, distance estimates for PNe appear to fall into two categories: a "short" scale advocated by groups such as Cahn & Kaler (1971), Kaler et al. (1990), and Phillips (2004) and a "long" scale tied to the results of Zhang (1995) and Giammanco et al. (2011). The short scale is supported by trigonometric parallaxes of PN central stars (e.g., Pottasch & Acker 1998; Harris et al. 2007; Benedict et al. 2009), although the relative proximity to the Sun for such objects makes them less than ideal for such an assessment. A more definitive test could be made by membership of a PN in a distant open cluster, but, as noted previously, the PN phase is relatively short-lived, more than 99% of open clusters capable of housing their progenitors have dissolved by the time they are old enough to produce one, and most cases examined so far are line-of-sight projections rather than physical associations (Majaess et al. 2007).

A new case of a planetary nebula and open cluster association was recently discovered by Bonatto et al. (2008) involving the planetary nebula Abell 8 (PN G167.0–00.9) with the cluster Bica 6. Abell 8 was discovered on Palomar Observatory Sky Survey images by Abell (1955, 1966), and the associated cluster was discovered by Bica (see Bonatto et al. 2008); its present designation is from the 2009 update of the open cluster catalog of Dias et al. (2002). Preliminary parameters for Bica 6 from 2MASS (Two Micron All Sky Survey) JHK_s data imply a cluster age of 1.0 ± 0.1 Gyr (Bonatto et al. 2008), indicating a progenitor star of less than ∼3 $M_\odot$. It is a sparse cluster with an as-yet-uncertain implied reddening and distance, which is a feature that might be resolved through a photometric and spectroscopic study at visible wavelengths. Presented here are new observations of that type, revealing interesting characteristics of the cluster and its embedded planetary nebula and strengthening the case for their association.

It is also noted here that the central star of Abell 8 appears to be double at far-infrared wavelengths, which is a characteristic not seen in the visual region. That point requires further study,

since the detection is at the brightness limits of the 2MASS survey.

2. OBSERVATIONS AND DATA REDUCTIONS

2.1. Photometric and Spectroscopic Observations

Low-dispersion CCD spectra (60 Å mm^{-1}) for bright members of Bica 6 were obtained in 2009 January and 2010 September using the Cassegrain spectrograph on the 1.85 m Plaskett telescope of the Dominion Astrophysical Observatory. The same telescope was also used in direct imaging mode to obtain broadband, all-sky, CCD, UBV photometry for the cluster in 2009 January, as well as CCD photometry on the Gunn system in 2010 February, with the latter to provide independent estimates for the magnitudes and colors of the planetary nebula's central star. Cousins system CCD $BV(RI)_C$ photometry was obtained in 2010 March for cluster stars brighter than $V = 18$ using the 0.35 m robotic telescope at Sonoita Research Observatory. The latter observations are tied to numerous standards (Landolt 1983, 1992) observed over a large range of air masses and have an external zero-point uncertainty of about 0.02 mag. A program of regular observation of the cluster in the Johnson V band was also made at the Abbey Ridge Observatory (Majaess et al. 2008) in order to search for variability among bright cluster members, but without positive detections to date.

2.2. Photometric Reductions

The optical UBV observations of Bica 6 were obtained on the nights of 2009 January 23/24 and 25/26 PST with the 1.85 m Plaskett telescope and E2V-1 CCD detector, with both nights being considered to be of photometric quality. The CCD chip (1024×2304 pixels binned 2×2) is too large to accommodate uniform illumination at the telescope focus, so the frames were trimmed to a usable size of 1020×1800 pixels before processing. The chip's image scale of $0.59''$ pixel^{-1} and frame size after trimming resulted in a surveyed field measuring $10' \times 17.7'$.

A selection of Landolt (1992) standard stars bracketing the air masses of the program fields and a standard field in NGC 2419 identified by Stetson (Canadian Astronomy Data Centre local projects) were used for the transformations. Since Stetson's observations consist of $BVRI$ only, photoelectric photometry from Racine & Harris (1975) was used to obtain standard U magnitudes for NGC 2419.

The images were bias-subtracted and flat-fielded using standard routines within IRAF. Absolute photometry was performed on all frames according to the usual procedure of point-spread function fitting using DAOPHOT and ALLSTAR, followed by aperture corrections and transformations to the standard system using routines provided by Stetson (2008, private communication). Because of concerns about the photometric stability of the two nights of observation, transformation equations initially were obtained by allowing the software to compute the solution

using individually determined zero points for the images. Good frames were selected on the basis of the zero points and the FWHM measurements of the stars, as well as visual inspection of the frames themselves. Since the quality of the nights proved to be somewhat uneven, a selection of local standards were used as well; the Sonoita photometry was used for those stars. A log of the DAO observations that were used in the analysis is given in Table 1. Note that, as a result of the preceding frame selection process, the program field air masses were not always bracketed by the standard ones.

The transformation equations used were of the form

$$v = V + a_0 + a_1 X + a_2(B - V)$$
$$b = B + b_0 + b_1 X + b_2(B - V)$$
$$u = U + c_0 + c_1 X + c_2(U - B),$$

where b, v, and u are the instrumental magnitudes; B, V, and U are the transformed magnitudes; X is the air mass; and the colors are the standard values. The transformation coefficients were obtained iteratively using least squares, with observations weighted according to the standard and observed photometric uncertainties and the residuals (observed minus actual). Typical weights ranged from 1.0 for residuals less than 0.022 to 0.10 for residuals of 0.042. Since the quality of the two nights differed, transformation coefficients for each night were obtained separately and kept for the rest of the calibration (a useful feature of the Stetson routines); the photometry from both nights was combined in the last step (weighted according to the quality of the data). The coefficients obtained are in Table 2. The average uncertainty (s.e.) per observation ranged from ±0.006 for V to ±0.029 for U.

Typical PSF-fitting uncertainties as determined by DAOPHOT and ALLSTAR ranged from δu, δv, and $\delta b \simeq \pm0.001$, ±0.001, and ±0.002 for instrumental magnitudes of u, b, and $v = 12$ to δu, δb, and $\delta v \simeq \pm0.013$, ±0.024, and ±0.027 for instrumental magnitudes of 16, for combined U, B, and V images of exposure times of 360 s, 180 s, and 90 s, respectively. Uncertainties for the adopted aperture corrections varied between ±0.0002 and ±0.0147, depending on the aperture, with a median value of about ±0.002. Uncertainties in the final transformed photometry are presented in Figure 1.

2.3. Spectroscopic Reductions and Spectral Classifications

The spectra were used to classify cluster stars on the MK system using standard techniques involving line strengths and line ratios in the blue-green spectral region (see Gray & Corbally 2009), as well as to derive radial velocities for the stars. A finder chart for the spectroscopically observed objects is presented in Figure 2, the continuum-flattened spectra are plotted in Figure 3, and Table 3 summarizes information for the stars, as well as for the central star of Abell 8. The stars are identified by their J2000 coordinates in the 2MASS catalog

TABLE 1
LOG OF DAO PHOTOMETRIC OBSERVATIONS

Date (UT)	Filter	Exp. time (s)	Air mass (start)
Bica 6			
2009 Jan 24	U	3 × 90	1.014
2009 Jan 24	U	3 × 360	1.017
2009 Jan 24	B	3 × 40	1.021
2009 Jan 24	B	3 × 180	1.026
2009 Jan 24	V	4 × 20	1.032
2009 Jan 24	V	3 × 90	1.037
2009 Jan 26	U	3 × 90	1.019
2009 Jan 26	U	3 × 360	1.015
2009 Jan 26	B	3 × 40	1.029
2009 Jan 26	B	3 × 180	1.024
2009 Jan 26	V	3 × 20	1.035
2009 Jan 26	V	2 × 90	1.032
PG 0220+132			
2009 Jan 24	B	3 × 240	1.242
2009 Jan 24	V	3 × 180	1.232
SA 101			
2009 Jan 24	U	1 × 90	1.517
2009 Jan 24	U	1 × 500	1.518
2009 Jan 26	U	1 × 90	1.435
2009 Jan 26	U	1 × 360	1.432
2009 Jan 26	B	2 × 40	1.542
2009 Jan 26	V	2 × 20	1.517
2009 Jan 26	V	2 × 90	1.518
PG0918+029			
2009 Jan 26	U	1 × 90	1.435
2009 Jan 26	U	1 × 360	1.432
2009 Jan 26	B	3 × 180	1.250
2009 Jan 26	V	1 × 20	1.440
2009 Jan 26	V	2 × 90	1.445
NGC 2419			
2009 Jan 24	U	2 × 90	1.198
2009 Jan 24	U	2 × 500	1.176
2009 Jan 24	B	3 × 60	1.250
2009 Jan 24	B	3 × 60	1.045
2009 Jan 24	B	2 × 240	1.220
2009 Jan 24	B	1 × 240	1.035
2009 Jan 24	V	3 × 30	1.297
2009 Jan 24	V	3 × 30	1.063
2009 Jan 24	V	2 × 180	1.281
2009 Jan 24	V	3 × 180	1.052
2009 Jan 26	U	2 × 90	1.016
2009 Jan 26	U	3 × 360	1.014
2009 Jan 26	U	2 × 500	1.319
2009 Jan 26	U	2 × 500	1.319
2009 Jan 26	B	1 × 40	1.022
2009 Jan 26	B	1 × 180	1.018
2009 Jan 26	B	1 × 240	1.411
2009 Jan 26	V	1 × 20	1.028
2009 Jan 26	V	2 × 90	1.024
2009 Jan 26	V	3 × 180	1.460
GD71			
2009 Jan 26	U	2 × 90	1.212
2009 Jan 26	U	2 × 360	1.196
2009 Jan 26	B	1 × 180	1.225
2009 Jan 26	V	2 × 20	1.246
G3-33			
2009 Jan 26	B	3 × 180	1.250
2009 Jan 26	V	3 × 90	1.263

Coefficient	Value	Coefficient	Value
	2009 Jan 24		2009 Jan 26
a_0	1.815 ± 0.002	a_0	1.750 ± 0.001
a_1	0.277 ± 0.006	a_1	0.183 ± 0.003
a_2	0.056 ± 0.003	a_2	0.068 ± 0.001
b_0	2.027 ± 0.005	b_0	2.053 ± 0.004
b_1	0.323 ± 0.015	b_1	0.574 ± 0.007
b_2	-0.149 ± 0.006	b_2	-0.162 ± 0.003
c_0	4.653 ± 0.006	c_0	4.630 ± 0.004
c_1	0.789 ± 0.027	c_1	0.650 ± 0.025
c_2	-0.079 ± 0.011	c_2	-0.075 ± 0.006

(Cutri et al. 2003), converted to degrees, and the numbering of Figure 2. The data include estimates of V, $B - V$, and $U - B$, with uncertainties of less than ± 0.01 mag for V and $B - V$ (except for the central star), spectral types assigned with reference to the MK spectral atlas and to Gray & Corbally (2009), reddening and distance modulus information inferred from the spectral classifications, and radial velocities derived from parabolic fits to the cores of reasonably strong, unblended lines in the spectra (54 lines per star, on average).

The precision of stellar radial velocities depends upon the spectral dispersion (e.g., Schneider et al. 1983), and for our wavelength-calibrated 60 Å mm^{-1} spectra, it is typically $\pm 10 \text{ km s}^{-1}$ or better (p.e.). The accuracy of the radial velocities obtained in this fashion is generally more secure. For example, a
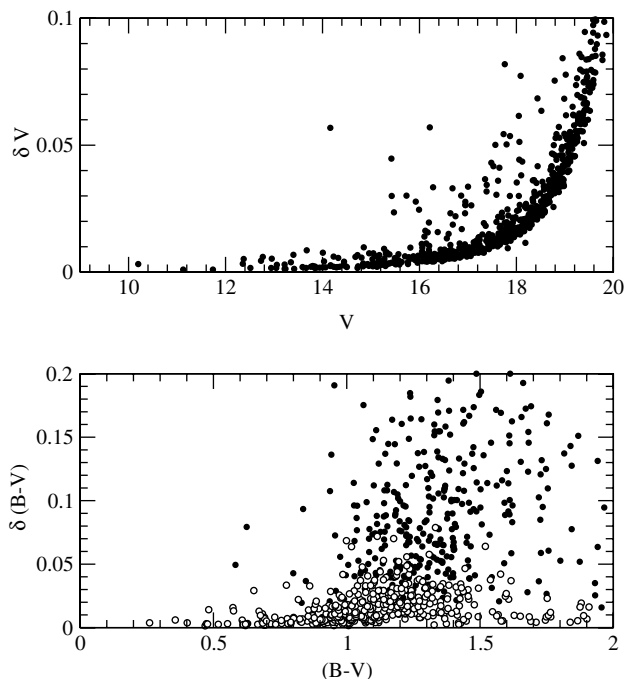

FIG. 1.—Photometric uncertainties plotted as functions of magnitude and color. Open circles denote stars detected on at least four B-band frames.
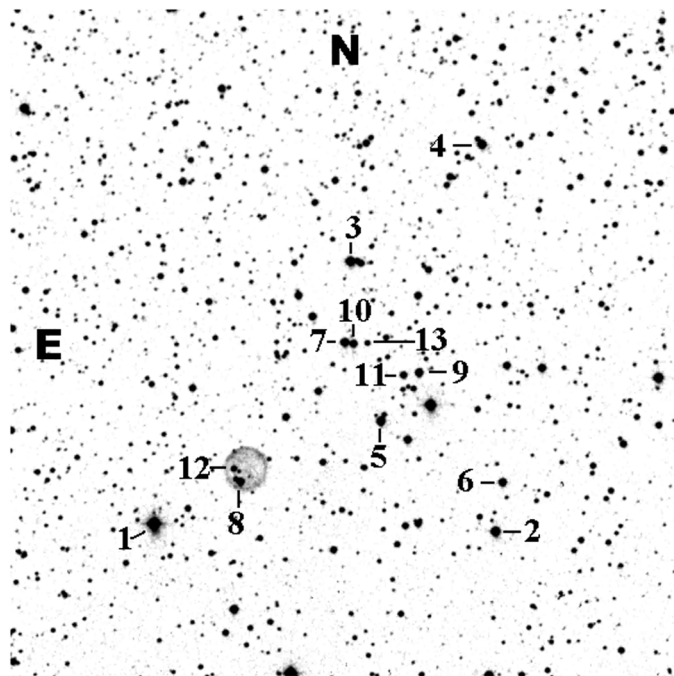

FIG. 2.—Finder chart for the 15′ diameter field of Bica 6 and Abell 8 centered on J2000 = 05:06:27.01, +39:11:01.7, derived from the POSS red image of the region, indicating stars observed spectroscopically in order of decreasing brightness.

spectral scan of a 103 Å mm^{-1} spectrogram for the Hyades spectroscopic binary HD 30869 by Turner et al. (1986) measured in such fashion yielded a velocity within 2 km s^{-1} of the actual value from only five unblended lines. Tests using a variety of CCD spectra obtained with the Plaskett telescope's Cassegrain spectrograph measured in similar fashion indicate no need for a zero-point adjustment.

Star 1 is HDE 277593, classified as B8e in the Henry Draper Extension. Our spectrogram does not extend to Hα, so we cannot confirm the emission-line nature of the star; higher Balmer series members are all in absorption. Moreover, the spectral lines display strong rotational broadening and also indicate a much earlier spectral type: B1 Vnn. Such a hot star appears anomalous, lying in the midst of a cluster of F-type and G-type giants. Yet its radial velocity is comparable with the velocities of other cluster members, which are about 60 km s^{-1} more positive than expected for standard Galactic rotation. The mean cluster velocity for the 11 stars of similar radial velocity is $57.1 \pm 1.2 \text{ km s}^{-1}$, where the cited uncertainty represents the standard error of the mean. The two deviant objects are star 7, conceivably a spectroscopic binary, given its similar reddening and distance modulus to other cluster stars, and star 13, which has a velocity consistent with Galactic rotation for a foreground star.

Table 3 includes information on the reddening and distance moduli of the stars, most of which are more luminous than
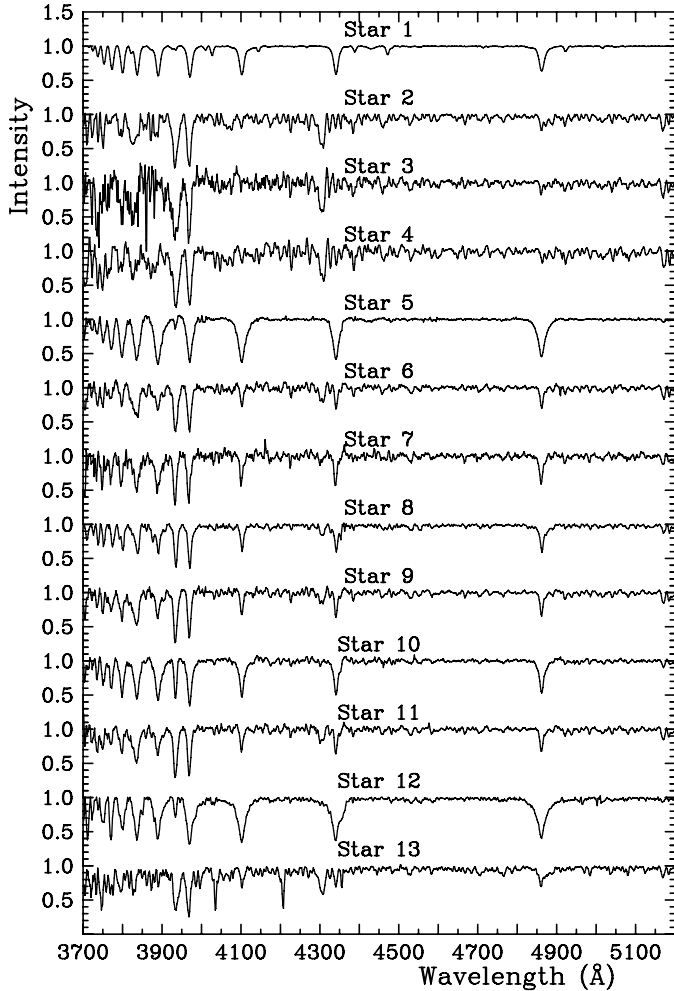
FIG. 3.—Montage of normalized spectra for Bica 6 stars identified in Fig. 2.

zero-age main-sequence (ZAMS) objects, where intrinsic colors were adopted from FitzGerald (1970), Kron (1978), and, for main-sequence stars, stellar atmosphere predictions for the colors of zero-age zero-rotation stars (Collins & Smith 1985) with a zero-point adjustment to match A0 stars (see Turner 1992) and absolute visual magnitudes from the compilation of Gray & Corbally (2009) in conjunction with an extension of the calibration of Turner (1980). A ratio of total-to-selective extinction of $R = A_V/E_{B-V} = 3.0 \pm 0.1$ and a reddening relation of slope $E_{U-B}/E_{B-V} = 0.75$ for early-type stars were found previously for fields lying at the Galactic longitude of Bica 6 (Turner 1976b) and were adopted here. The variation of apparent distance modulus, $V - M_V$, with color excess, E_{B-V}, for stars in Table 1 is consistent with such a result (see § 3).

2.4. Photometric Standardization

As noted previously, the direct images of Bica 6 from the DAO were calibrated using comparable images of standard stars

observed at air masses similar to those for Bica 6. For consistency, minor adjustments were made to the BV magnitudes to improve the match to the all-sky CCD $BV(RI)_C$ photometry from the Sonoita images. A similar procedure was used for the initial calibration of the U-band images, namely, by reference to U magnitudes for standard stars. However, most current CCD-telescope-filter combinations produce very poor matches to the wavelength sensitivity of the Johnson U filter (see Turner 2011), and in such cases the calibration of U magnitudes and $U - B$ colors can be nonlinear and possibly multivalued (Moffat & Vogt 1977; Cousins & Caldwell 2001). In fact, the initial UBV color-color diagram constructed for cluster stars displayed characteristics indicating systematic effects in the U data.

Removal of such effects from the final data set was done as follows. The $BV(RI)_C$ colors for Bica 6 stars plotted in Figure 4 indicate that the only unreddened objects in the field are late-type stars and one or two likely early A-type stars. The majority of stars in the sample are reddened by about $E_{B-V} \simeq 0.5$. For spectroscopically observed stars, one can relate the spectral type of the star to tabulated intrinsic colors (e.g., FitzGerald 1970) to calculate the correction, $\delta(U - B)$, to the initially observed $U - B$ color, which is required to make the computed color excesses E_{U-B} and E_{B-V} fit the accepted reddening relation for the field, adjusted in the case of the cooler stars for the color dependence of color excesses and reddening slope (e.g., Fernie 1963). For a few stars it was possible to identify them from Figure 4 as unreddened main-sequence stars from their faintness and $BV(RI)_C$ colors, thereby indicating the correction to $U - B$ needed to make their colors fit the intrinsic color-color relation for dwarfs. Finally, the field reddening for spectroscopically observed stars varies relatively smoothly across the field, so some of the fainter stars lying within roughly 30″ of them and indicated to be reddened from their $BV(RI)_C$ colors were assumed to share the same reddening, as an approximation, thereby allowing additional corrections to $U - B$ to be calculated.

The dependence of the derived corrections for the stars is plotted as a function of observed $B - V$ color in Figure 5, producing a reasonably well defined dependence matched to a best-fitting polynomial. Normally, such corrections are spectral-type-dependent (see Moffat & Vogt 1977), but most stars in the Bica 6 field are reddened by similar amounts, which are not large, so a simple color dependence appears to be appropriate. The adopted color dependence $\delta(U - B)$ shown in Figure 5 was therefore applied to all observed stars, except very red objects with $B - V \geq 1.45$, for which a constant correction of $+0.15$ produced more reasonable results.

The effectiveness of such a procedure can be judged from Figure 6, which plots the UBV color-color diagram for the 391 stars in the final adjusted data set that have full UBV coverage. The colors for cluster stars are a good match to the intrinsic relation reddened by $E_{B-V} = 0.42$, which represents the mean color excess for the field. According to the results of Figure 5,

TABLE 3
Spectroscopic and Photometric Data for Bright Bica 6 Stars

Star	R.A. (2000)	Decl. (2000)	V	B − V	U − B	Sp.T.	B − V₀	E_{B-V} (B0)	V − M_V	V₀ − M_V	V_R (km s⁻¹)	ΔV_R (km s⁻¹)	Lines
1[a]	76.70364	39.11653	10.20	0.26	−0.52	B1 Vnm	−0.27	0.53	12.33	10.73	+61	±6	24
2	76.53968	39.11315	12.35	1.43	+1.07	G6 II-III	+0.92	0.56	12.85	11.18	+55	±10	60
3	76.60863	39.21426	12.51	1.37	+1.24	G8 III	+0.95	0.47	12.21	10.81	+53	±10	56
4	76.54565	39.25783	12.69	1.37	+1.30	G7 III	+0.94	0.46	12.39	11.02	+56	±6	50
5	76.59442	39.15476	12.73	0.36	+0.12	B9.5 IV	−0.03	0.39	12.43	11.24	+61	±7	56
6	76.53616	39.13146	12.94	0.76	+0.26	F7 III	+0.50	0.27	12.34	11.52	+55	±7	63
7	76.61181	39.18389	12.95	0.78	+0.33	F2 III	+0.36	0.44	12.35	11.04	(+23)	±11	62
8	76.66211	39.13222	13.05	0.71	+0.23	F3 III	+0.38	0.36	12.45	11.38	+62	±11	45
9	76.57605	39.17258	13.06	0.78	+0.31	F5 III	+0.41	0.39	12.36	11.19	+51	±8	68
10	76.60746	39.18347	13.24	0.62	+0.42	F0 IV	+0.31	0.33	11.54	10.56	+59	±6	26
11	76.58347	39.17167	13.88	0.69	+0.41	F6 IV	+0.46	0.25	11.68	10.93	+54	±6	73
12	76.66512	39.13706	14.72	0.67	+0.43	A3 V	+0.09	0.59	12.72	10.94	+60	±5	45
13	76.60073	39.18366	15.59	0.99	+0.34	G0 V:	+0.59	0.43	11.99	10.71	(−2)	±6	96
CS	76.65983	39.135833	19.93	0.15	...	...	(−0.38)	(0.49)	...	(11.02)	...	...	...
Average	...	...	...	...	...	...	...	0.42	...	11.02	+57	...	...
s.e.	...	...	...	...	...	...	...	±0.03	...	±0.08	±1	...	...

[a] HDE 277593, B8e.

FIG. 6.—Color-color diagram, $U - B$ vs. $B - V$, for stars in Bica 6, from the final adjusted photometry. The solid curve represents the intrinsic relation for main-sequence stars, and the narrow curve the same relation reddened by $E_{B-V} = 0.42$. An arrowed line shows the effects of interstellar reddening on the colors for $E_{B-V} = 0.5$.
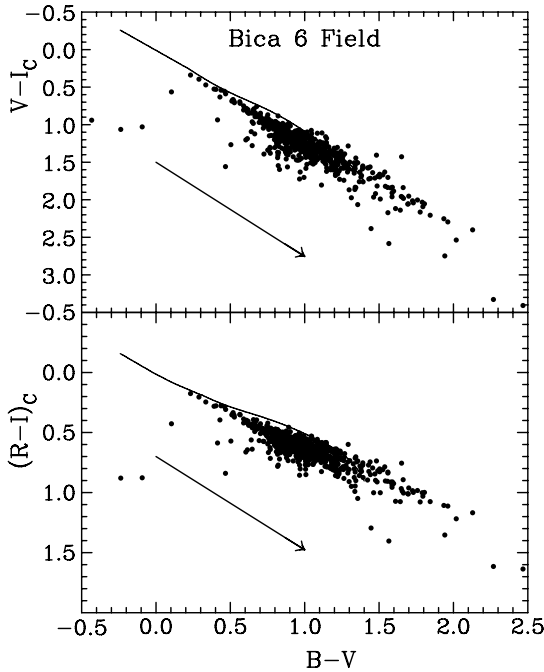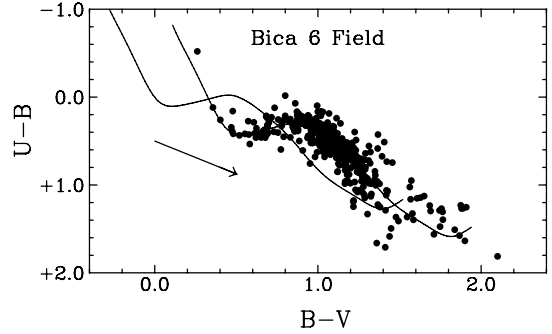

FIG. 4.—$V - I_C$ and $(R - I)_C$ colors as a function of $B - V$ for stars in the Bica 6 field relative to the intrinsic relations for dwarfs (curved relations). Arrowed lines depict the effects of interstellar reddening for $E_{B-V} = 1.00$.

the uncertainties in the adjusted $U - B$ colors may be as large as ± 0.10, although for most stars they are probably not much larger than ± 0.05. Within such limits, the color-color data of Figure 6 are well matched to the reddened intrinsic relation over the entire range of likely spectral types for the stars, from B-type stars to M-type stars.

The final corrected UBV observations for Bica 6 stars, as well as $(RI)_C$ data, are on deposit at the WEBDA Open Cluster Database,[3] and identify the 2000 coordinates for each star, along with the observed values of V, $B - V$, $U - B$, $V - R_C$, $V - I_C$, and $(R - I)_C$ and their uncertainties. The complete table of CCD data for almost 800 observed stars is too large to publish here.

3. PARAMETERS OF BICA 6

Figure 7 is a color-magnitude diagram for the complete data set of observed Bica 6 stars, with no elimination of foreground or background stars. Included is the ZAMS relation from Turner (1976a, 1979) reddened by $E_{B-V} = 0.42$ for $V - M_V = 12.28$, along with a theoretical isochrone for $\log t = 9.0$ from Meynet et al.(1993) matched to the same parameters. The parameters are in very close agreement with the results obtained by Bonatto et al. (2008) from 2MASS JHK_s data. A variety of more recently published isochrones could have been plotted for comparison, with nearly identical results. Those of Meynet et al. (1993) were employed because they appear to provide slightly better fits to the observational data for stars in open clusters than is the case with some others (see Turner 2011).

An independent solution for Bica 6 was attempted with the 2MASS observations (Cutri et al. 2003) using the intrinsic JHK_s relations of Turner (2011). JHK_s data for stars lying within 6′ of the center of Bica 6 cited by Bonatto et al. (2008) are plotted in Figure 8, along with the intrinsic relations of Turner (2011). The data were separated according to the cited uncertainties in the magnitudes into a high-quality group, $\sigma \leq \pm 0.06$, and a low-quality group with larger uncertainties. It was difficult to establish the reddening uniquely, either because of large scatter in the data or because of differential reddening in the field, although there is a reasonably good match of the data to $E_{J-H} = 0.124$, corresponding to the average

FIG. 5.—Correction for $U - B$ colors as a function of $B - V$ for stars observed spectroscopically (*filled circles*) and stars that are either unreddened or reddened as their nearby spectroscopic neighbors (*open circles*). The plotted gray relation was adopted to adjust the CCD colors to the Johnson system.

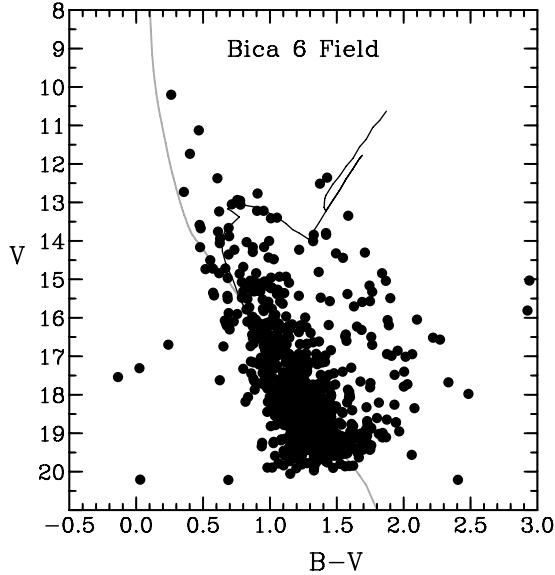[3] See http://www.univie.ac.at/webda/.

FIG. 7.—Color-magnitude diagram for Bica 6 from the full data set. The gray curve is the ZAMS for $E_{B-V} = 0.42$ and $V - M_V = 12.28$, and the black curve is a theoretical isochrone for $\log t = 9.0$ from Meynet et al. (1993) for the same parameters.

reddening of $E_{B-V} = 0.42$ obtained for the UBV data. For that reddening the apparent distance modulus is $J - M_J = 11.32$ from ZAMS fitting, coincident with the distance modulus of $V - M_V = 12.28$ used with the BV data in Figure 7. There is also a close match of a $\log t = 9.0$ isochrone to the JHK_s data, as noted by Bonatto et al. (2008), although the model isochrone used in Figure 8 is an independent relation adapted from Meynet et al. (1993) (see Turner 2011).

The existence of differential reddening across the field of Bica 6 is evident from the reddenings for spectroscopically observed stars (Table 3), as well as from sizeable scatter in the UBV and 2MASS colors for cluster stars (Figs. 6 and 8) and visual inspection of images of the field. There is a noticeable increase in the visual extinction on the southwest side of the field, according to an apparent decrease in star densities there, and that is confirmed by the derived color excesses of stars in the region. As a consequence, the final parameters for Bica 6 were established from a variable-extinction analysis of the UBV observations for cluster stars (see Turner 1976a, 1976b). Stars with full UBV coverage were therefore individually dereddened to the intrinsic relation for main-sequence stars in Figure 6, color excesses were adjusted to equivalent values for a B0 star using the relationship of Fernie (1963), and apparent distance moduli were calculated using ZAMS values of M_V from Turner (1976a, 1979). The results are shown in Figure 9, along with the apparent distance moduli for spectroscopically observed stars in Table 3.

An alternate method to dereddening the data is possible using $BVRI_C$ or other infrared colors, but such an approach
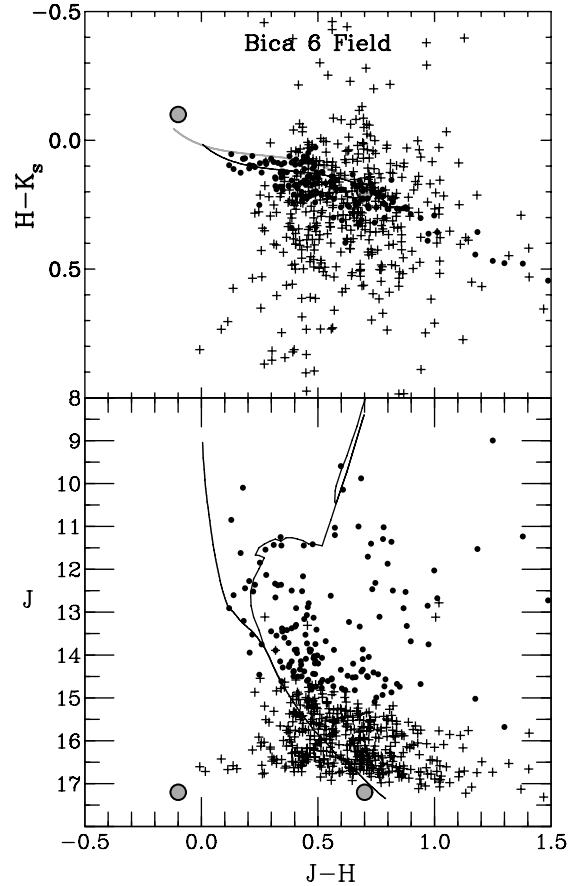

FIG. 8.—2MASS color-color diagram, $H - K_s$ vs. $J - H$ (top), and color-magnitude diagram, J vs. $J - H$ (bottom), for stars within 6′ of the center of Bica 6, from observations by Cutri et al. (2003). Top: Intrinsic color-color relation for main-sequence stars is plotted as a gray curve, and a solid black curve is the same relation reddened by $E_{J-H} = 0.124$ ($E_{B-V} = 0.42$). Bottom: ZAMS is plotted as a black curve for the same reddening and $J - M_J = 11.32$ ($V - M_V = 12.28$), and the gray curve is an isochrone for $\log t = 9.0$. Filled circles represent data with uncertainties smaller than ±0.06, plus signs represent data with larger uncertainties, and gray circled points are estimates for the two stars near the center of Abell 8.

in this instance would result in greater uncertainties in the derived color excesses. Most of the stars in the field are of apparently late spectral type, for which $BVRI_C$ reddening lines run nearly parallel to the intrinsic color relations for dwarfs (see Turner et al. 2011 and Fig. 4). Attempts to infer intrinsic colors for stars in the observational sample would therefore produce color excesses E_{B-V} of larger uncertainty than those generated from analysis of the UBV observations.

An initial concern with such an approach was the possibility that large scatter in the $U - B$ colors might produce biased results. The effects of random photometric errors on variable-extinction analyses of O-type, B-type, and A-type stars were investigated previously by Turner (1976a), and it is a simple matter to extend the results to the GK dwarfs dominating the
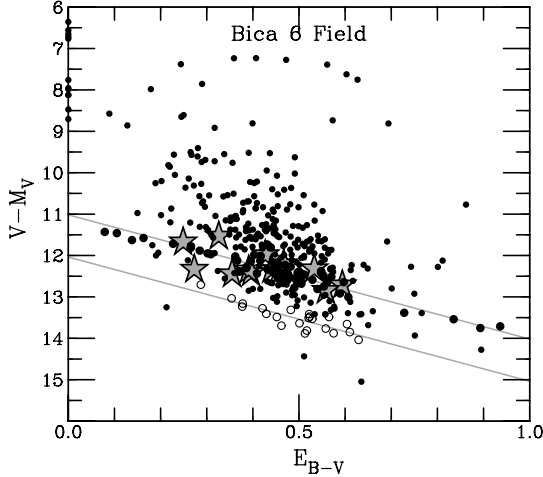
FIG. 9.—Variable-extinction diagram for stars in the Bica 6 field (*filled circles*), including likely ZAMS members (*large filled circles*), likely ZAMS stars for the background group (*open circles*), and spectroscopic distance moduli for stars in Table 1 (*gray stars*). The two gray lines are $R = 3.0$ relations for the Bica 6 cluster (*top*) and the background group (*bottom*).

field of Bica 6. As a consequence, we expect the determination of $R = A_V/E_{B-V}$ for cluster stars to be biased toward a value of $R = 1.9$, with a total spread in color excesses E_{B-V} approximating ∼0.2. The data of Figure 9 are at complete variance with such expectations. There is no apparent bias toward a value of $R \simeq 2$, and the spread of color excesses is more than twice as large as expected. There are also many unreddened stars in the field. Given the generally consistent trends of the data in both Figures 6 and 9 to what is typical of the scatter in cluster color-color and variable-extinction diagrams for good-quality data (see Turner 1976a, 1976b), it appears that the uncertainties in the derived $U - B$ colors amount to ±0.10 only in extreme cases. The true scatter for most cluster stars appears to be much smaller, as noted earlier.

The data of Figure 9 fall into five distinct groups: (1) unreddened foreground stars with apparent distance moduli of $V_0 - M_V \leq 8.7$, indicating that the dust clouds creating much of the extinction in the Bica 6 field lie at distances of $d \simeq 550$ pc; (2) reddened foreground stars more distant than 550 pc with color excesses ranging from 0.2 to 0.9 and apparent distance moduli of 7–12; (3) three apparently reddened background objects (or stars with anomalous data) with true distance moduli of $V_0 - M_V \geq 12.5$; (4) a group of 64 stars with $V_0 - M_V \simeq 11$ and color excesses ranging from 0.08 to 0.94, most of which are likely ZAMS members of Bica 6; and (5) a group of 22 stars with $V_0 - M_V \simeq 12$ and color excesses ranging from 0.29 to 0.63 that appear to be ZAMS members of a group lying background to Bica 6. All of the stars in group 5 lie on the northeast side of the field and may be associated with a sparse, perhaps dissolved, cluster of faint stars that appears to lie

in that region. The data for stars in group 5 were analyzed using least-squares and nonparametric techniques, yielding a value of $R = A_V/E_{B-V} = 3.05 \pm 0.31$ s.e. and $V_0 - M_V = 12.01 \pm 0.15$ s.e., corresponding to a distance of 2.56 ± 0.18 kpc (s.d.).

The data for stars in the more populous group 4 were also analyzed using least-squares and nonparametric techniques, which yielded a value of $R = A_V/E_{B-V} = 2.99 \pm 0.13$ s.e. and $V_0 - M_V = 11.02 \pm 0.06$ s.e., corresponding to a distance of 1.60 ± 0.11 kpc (s.d.). The values of R derived for both groups agree with prior expectations ($R = 3.0$, § 2.3) for the characteristic properties of dust clouds lying in the direction of Bica 6 (Turner 1976b), and the implied distance of ∼550 pc to the dust complex along the line of sight matches independent results by Neckel & Klare (1980) for the distribution of dust along adjacent Galactic sight lines. The latter results also indicate that there is no additional reddening in this direction for another 2 kpc or so, presumably implying that the interarm region between the local Cygnus arm and the Perseus structure is relatively free of dust and extinction. That would explain why there is no obvious separation of groups 4 and 5 in Figure 9 in terms of color excess, E_{B-V}. The stars in both groups have been reddened by the dust associated with a complex lying well foreground to them.

It is worth pointing out that results such as those presented here appear to be typical of what is found in other Galactic star fields associated with open clusters (Turner 1994). Galactic dust complexes appear to be spatially restricted around the Sun (Neckel & Klare 1980), producing interstellar reddening and extinction of differing amounts for all stars lying beyond a dust complex or between individual complexes. The notion of interstellar reddening increasing monotonically with distance from the Sun is incorrect. In most directions the reddening is produced in one or more dust clouds lying along the line of sight, with the reddening for individual stars reflecting both the number of dust clouds lying between the star and the Sun and the amount of extinction occurring in each cloud along the line of sight to the star. In the case of the Bica 6 field, there appears to be only one dust complex detected to the limits of the survey, and it is located ∼550 pc distant.

Spectroscopically observed stars confirm the results of the variable-extinction analysis. The derived mean intrinsic distance modulus for stars in Table 3 is $V_0 - M_V = 11.02 \pm 0.08$ s.e., which is identical to what was found from ZAMS fitting, regardless of questions about the membership status of individual stars. The corresponding distance of 1.60 ± 0.06 kpc agrees with the value of 1.7 ± 0.1 kpc obtained by Bonatto et al. (2008) for Bica 6 using an independent main-sequence calibration. The close agreement of UBV, JHK_s, and spectroscopic distance estimates for Bica 6 provides a solid foundation for the distance of the cluster. The reddening is also confirmed to be differential across the face of the cluster, but lies mainly in the range from 0.2 to 0.6 in E_{B-V}, averaging 0.42 in E_{B-V}.

4. CLUSTER MEMBER ABELL 8

Some of the observed parameters of Abell 8 (PN G167.0–00.9) are relatively poorly established (Kaler 1983; Cahn et al. 1992), but sufficient to permit estimates of reddening from the Hβ/radio flux method (Milne & Aller 1975; Cahn 1976; Bianchi & Grewing 1985) or the Balmer line method (Osterbrock & Ferland 2006). The color excess is $E_{B-V} = 0.55 \pm 0.45$ when one combines the 1.4 GHz flux density measured by Condon & Kaplan (1998) with the Hβ flux estimated by Kaler et al. (1990) and Cahn et al. (1992), with the generous uncertainty resulting from propagation of the large relative uncertainties in the input quantities. Estimates for the reddening from the Balmer decrement (Cahn & Kaler 1971; Ali 1999; Philips et al. 2005; Giammanco et al. 2011) in conjunction with the conversion factor of Majaess et al. (2007) imply values of $E_{B-V} = 0.51, 0.44, 0.42$, and 0.47, respectively, with expected uncertainties for the latter of the order of ± 0.08 (e.g., Osterbrock & Ferland 2006). The reddening estimates are summarized in Table 4, along with independent estimates for radial velocity and distance.

An independent estimate is possible from the space reddening information obtained from the variable-extinction analysis presented here. The reddening of stars in Bica 6 and near Abell 8 (Fig. 10) suggests the existence of internal reddening within the nebula itself. Stars near the planetary nebula have color excesses of $E_{B-V} = 0.37 \pm 0.01$ (two in front), 0.59 (behind), and 0.53 (off west limb), implying an internal reddening of $E_{B-V} \simeq 0.22$. Such a result appears reasonable given possible excess reddenings for PNe associated with dust produced during evolution on the asymptotic giant branch for their progenitor stars (see Majaess et al. 2007). The implied reddening of the central star is therefore $E_{B-V} = 0.48 \pm 0.05$, where the uncertainty reflects the full spread in internal reddening inferred for the planetary. A similar value of $E_{B-V} = 0.53 \pm 0.05$ is obtained by adopting an intrinsic $B - V$ color of -0.38 from Kaler & Feibelman (1985) with the observed color from Table 5. The various estimates of reddening are remarkably consistent, yielding a mean value of $E_{B-V} = 0.49 \pm 0.02$, adopted here.

The measured radial velocity of Abell 8 is 58.2 ± 6.5 km s^{-1} (Schneider et al. 1983; Durand et al. 1998), according to measurements from low-quality spectra by Purgathofer & Perinotto (1981). That agrees with the radial velocity for Bica 6 members of 57.1 ± 1.2 km s^{-1} (Table 3). The good agreement in the estimates of reddening and radial velocity for the planetary nebula with values obtained for stars in Bica 6 provides reasonably good evidence for their physical association, although the case from reddening alone is clearly weak, given that it results from dust clouds lying well foreground to Bica 6.

Estimates for the distance to Abell 8 (PN G167.0–00.9) are typically linked to inferences about its reddening, but vary from short values of 1.67 kpc (Kaler et al. 1990) and 1.78 kpc (Cahn & Kaler 1971; Phillips 2004) to long values of 3.23 kpc (Zhang 1995) and 5.5 kpc (Giammanco et al. 2011) according to the methodology used, as indicated in Table 4. The former are very close to the distance of 1.60 ± 0.11 kpc obtained here for Bica 6, thereby favoring the short scale of planetary nebula distances.

The IPHAS result (Giammanco et al. 2011) is significantly different and appears to imply a reddening-distance relation

TABLE 4
DEDUCED PARAMETERS FOR ABELL 8 AND BICA 6

Parameter	Abell 8	Source	Bica 6	Source
V_R	58.2 ± 6.5 km s^{-1}	Purgathofer & Perinotto (1981)	57.1 ± 1.2 km s^{-1}	This article
E_{B-V}	0.51[a]	Cahn & Kaler (1971)	0.42 ± 0.20[e]	This article
E_{B-V}	0.44[a]	Ali (1999)	...	...
E_{B-V}	0.42[a]	Philips et al. (2005)	...	...
E_{B-V}	0.47[a]	Giammanco et al. (2011)	...	...
E_{B-V}	0.55 ± 0.45[b]	This article	...	...
E_{B-V}	0.48 ± 0.05[c]	This article	...	...
E_{B-V}	0.53 ± 0.05[d]	This article	...	...
Distance	2.05 kpc	Abell (1966)	1.60 ± 0.11 kpc	This article
Distance	1.78 kpc	Cahn & Kaler (1971)	...	...
Distance	2.66 kpc	Kaler (1983)	...	...
Distance	2.60 kpc	Maciel (1984)	...	...
Distance	1.67 kpc	Kaler et al. (1990)	...	...
Distance	1.86 kpc	Cahn et al. (1992)	...	...
Distance	3.23 kpc	Zhang (1995)	...	...
Distance	1.78 kpc	Phillips (2004)	...	...
Distance	5.50 kpc	Giammanco et al. (2011)	...	...

[a] Balmer decrement method.
[b] Hβ/radio flux method.
[c] Space reddening.
[d] Spectroscopic/photometric reddening.
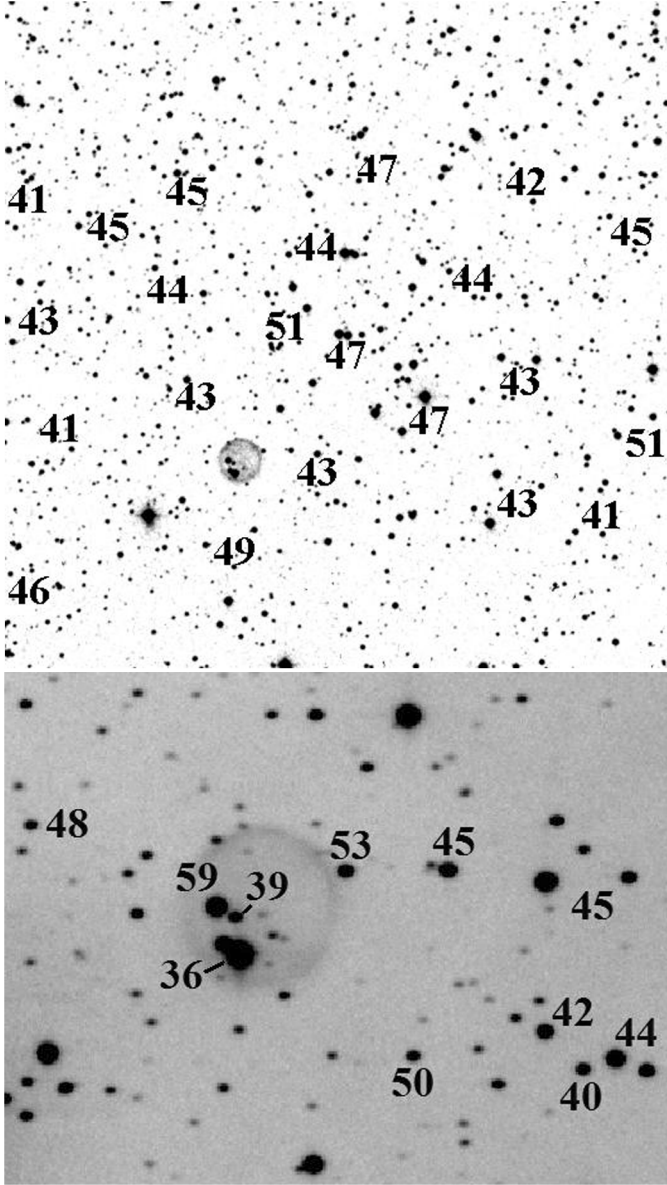[e] Range for most cluster members.

FIG. 10.—Derived space reddenings (*numerals in black*) for Bica 6 stars for the field of Fig. 2 (*top*) and in the vicinity of Abell 8 (*bottom*), with reddenings cited in units of 0.01 magnitude without the decimal. The reddenings for Bica 6 stars represent group means for clumps of six–eight stars in the same direction, and those for Abell 8 are individual color excesses.

TABLE 5

CENTRAL STAR OF ABELL 8

V	$B - V$	Source
19.89	0.15	This article (*BV* photometry)
19.99	0.10	This article (Gunn system photometry)
19.9	0.2	POSS; Abell (1966); Kaler et al. (1990)
19.93	0.15	Mean values

from IPHAS photometry for stars in this field that deviates markedly from results found here and by Neckel & Klare (1980). As noted earlier, interstellar reddening is difficult to correlate exactly with distance in the Galactic plane, given that it appears to arise mainly in distinct dust clouds along Galactic sight lines (see Turner 1994), and that may help to explain the discrepancy in this case. Note that the discrepancy is in distance only; the color excesses found for Abell 8 agree quite closely (Table 4).

The evidence for a physical association between Abell 8 and Bica 6 is particularly strong for the radial velocity observations, since the expected heliocentric velocity from Galactic rotation for an object 1.6 kpc distant at $\ell = 167°$ is ~ 60 km s^{-1} more negative. It would be highly unusual to have two spatially adjacent objects sharing such unusual Galactic orbits if they were not physically associated. Certainly, according to the criteria of Majaess et al. (2007), Abell 8 is a likely member of Bica 6.

5. EVOLUTIONARY CONSIDERATIONS

A selection of 114 stars in the Bica 6 field were identified as potential or likely cluster members according to the star counts of Bonatto et al. (2008), the radial velocity data (Table 3), their reddening, and inferred location in the color-magnitude diagram (Figs. 7 and 8). The colors and magnitudes were corrected individually for the effects of interstellar reddening and extinction, and the resulting extinction-corrected color-magnitude diagram
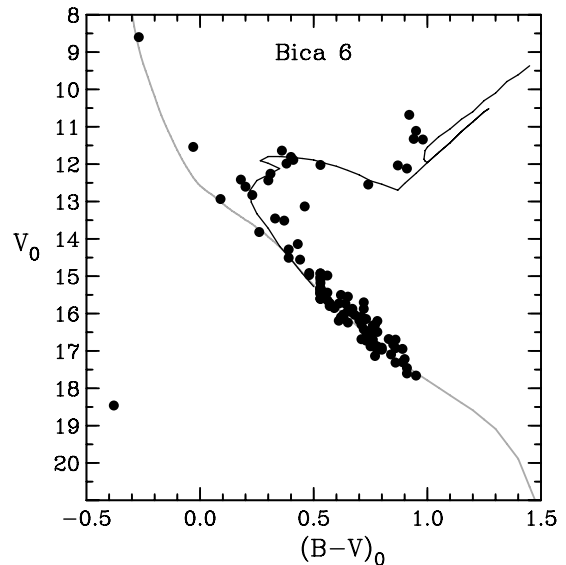

FIG. 11.—Color-magnitude diagram for likely and potential members of Bica 6, corrected for the effects of interstellar reddening and extinction for individual stars. The gray curve represents the ZAMS for $V_0 - M_V = 11.02$, and the black curve is an isochrone for $\log t = 9.0$. The central star of Abell 8 is the point at the lower left.

is shown in Figure 11. As is the case with the JHK_s data (Fig. 8 and Bonatto et al. 2008), the best isochrone fit is for $\log t = 9.0$.

In the evolutionary models of Meynet et al. (1993), stars reaching the terminal stages of evolution on the main sequence for $\log t = 9.0$ have masses of ~ 2.1 $M_\odot$, as is also the case for stars on the red giant branch of Bica 6 according to the VandenBerg et al. (2006) isochrones (not shown). The progenitor of Abell 8 (PN G167.0–00.9) must therefore have been a more massive B-type dwarf originally, perhaps up to ~ 2.3 $M_\odot$ ($\sim B9.5$ V spectral type). The implied current mass of ~ 0.6 $M_\odot$ for the central star of Abell 8 and ~ 0.55 $M_\odot$ for the nebular matter (Kaler 1983; Kaler et al. 1990) fall short of the progenitor star's original mass, implying extensive mass loss during the asymptotic giant branch phase of the star to fully account for the mass budget. The excess reddening for Abell 8 found here from space reddenings for spatially adjacent stars is consistent with such a picture.

Our various photometric estimates for the brightness of the blue central star of Abell 8 (Table 5) include eye estimates (e.g., Perek & Kohoutek 1967) from the Palomar Observatory Sky Survey (POSS), as well as our own estimates made from image diameters measured on the POSS II images and calibrated using similar measurements for adjacent stars of known magnitude (the present photometry). In conjunction with the field reddening of Table 4 and the derived distance to Bica 6, the data imply an absolute magnitude of $M_V = +7.44 \pm 0.16$ for the central star and a linear diameter for the PN of 0.47 ± 0.03 pc, consistent with the advanced evolutionary state of the planetary nebula and the star's location toward the cool end of the PN's central-star cooling sequence (Kaler 1983; Kaler et al. 1990). For comparison purposes, a distance of 5.5 kpc for Abell 8 (Giammanco et al. 2011) would imply an absolute magnitude of $M_V = +4.76$ for the central star and a linear diameter for the PN of 1.60 pc, which are parameters that are incompatible with each other. The former value is typical of a luminous central star that has only recently entered the PN stage (Benedict et al. 2009), while the latter value is large even for a highly evolved PN (Zhang 1995).

Our data for cluster stars suggest that the central star of Abell 8 should have a far-infrared brightness of roughly $J \simeq 20$, well beyond the magnitude cutoff of the online photometry for the 2MASS survey near $J = 17$, yet an image appears in the survey at $J \simeq 17.2$ at the proper location. By comparison, the star's optical brightness is near the limit of our imaging (see Figs. 2 and 10). It is conceivable that the infrared brightness of the object reflects emission from circumstellar dust, but additional observations are needed to assess such a possibility, as well as to confirm the results. The JHK_s data otherwise appear consistent with expectations for a blue central star, since the estimated $J - H$ and $H - K_s$ colors are -0.1 and -0.1, respectively.

Although the star is single at optical wavelengths, it appears to be double in 2MASS images. The companion lies $\sim 2''$ east of the central star and is of identical brightness in the J band, being brighter at H and K_s. Its estimated $J - H$ and $H - K_s$ colors are $+0.7$ and $+0.2$, respectively. The companion is undetected in optical images. Both stars fit nicely into the cluster color-color and color-magnitude diagrams for 2MASS photometry (Fig. 8), with the companion as an M dwarf, implying that the two stars may form a wide physical binary system, as well as a close optical double. The symmetrical shape of Abell 8 has been taken as evidence for a single progenitor central star by Soker (1997), which does not necessarily contradict such arguments.

Likely and potential cluster members in Figure 11 fit the 10^9 yr isochrone reasonably well, including the diagnostic "hook" in the models, providing some support for the isochrones used here. Yet there are three cluster stars lying blueward of the inferred main-sequence turnoff: star 1 (HDE 277593), B1 Vnn; star 5, B9.5 IV; and star 12, A3 V. All three are radial velocity members and, in the case of stars 5 and 12, closely fit the canonical description of blue stragglers. Star 1 is less easily explained, since its implied mass as a normal main-sequence star would be ~ 9–10 $M_\odot$, which is several times the turnoff point mass of the cluster. An intriguing possibility is that the star, if it is indeed a cluster member, is a post-asymptotic giant branch (AGB) object caught in the act of evolving into a planetary nebula. One other example of a post-AGB object, LS II + 34°26 = V1853 Cyg (Parthasarathy 1993), appears spectroscopically like a less-evolved object in blue-green spectra (Turner 1983, 2003; Turner & Drilling 1984), except for Balmer line emission. Star 1 may be a less extreme example of the phenomenon, given that it is not an IRAS source (see Parthasarathy 1993; Turner 2003). The difference between its original temperature classification as B8 and its present classification as B1 may, like LS II + 34°26, be indicative of rapid evolutionary changes (Turner 2003).

6. SUMMARY

Abell 8 (PN G167.0–00.9) is a very good case of a planetary nebula belonging to an open cluster, according to the spectroscopic and photometric results presented here. The inferred properties of the PN as a cluster member therefore provide useful empirical tests of the luminosities of PN central stars, as well as the PN distance scale. In the case of the latter, the implied distance of Abell 8 is consistent with the short PN distance scale, and at variance with results implied by advocates of the long distance scale. More intriguing, however, is the cluster Bica 6 itself, since it appears to contain stars in a variety of evolutionary states associated with the evolution of main-sequence stars to their eventual fate as white dwarfs. In addition to the PN and its central star, additional likely cluster members include standard F-type and G-type giants evolved from the main sequence, two likely blue stragglers, and one star, star 1 (HDE 277593), that may be a post-AGB star evolving toward the PN state. Future additional spectroscopic and photometric observations of cluster stars would appear to be justified.

REFERENCES

Abell, G. O. 1955, PASP, 67, 258

———. 1966, ApJ, 144, 259

Ali, A. 1999, NewA, 4, 95

Acker, A. 1978, A&AS, 33, 367

Acker, A., Fresneau, A., Pottasch, S. R., & Jasniewicz, G. 1998, A&A, 337, 253

Benedict, G. F., McArthur, B. E., & Napiwotzki, R., et al. 2009, AJ, 138, 1969

Bianchi, L., & Grewing, M. 1985, in IAU Symp. 111, Calibration of Fundamental Stellar Quantities (Dordrecht: D. Reidel), 603

Bonatto, C., Bica, E., & Santos, J. F. C., Jr. 2008, MNRAS, 386, 324

Cahn, J. H. 1976, AJ, 81, 407

Cahn, J. H., & Kaler, J. B. 1971, ApJS, 22, 319

Cahn, J. H., Kaler, J. B., & Stanghellini, L. 1992, A&AS, 94, 399

Collins, G. W., II, & Smith, R. C. 1985, MNRAS, 213, 519

Condon, J. J., & Kaplan, D. L. 1998, ApJS, 117, 361

Cousins, A. W. J., & Caldwell, J. A. R. 2001, MNRAS, 323, 380

Cutri, R. M., et al. 2003, 2MASS All-Sky Catalog of Point Sources, NASA/IPAC Infrared Science Archive, http://irsa.ipac.caltech.edu/applications/Gator

Dias, W. S., Alessi, B. S., Moitinho, A., & Lépine, J. R. D. 2002, A&A, 389, 871

Durand, S., Acker, A., & Zijlstra, A. 1998, A&AS, 132, 13

Fernie, J. D. 1963, AJ, 68, 780

FitzGerald, M. P. 1970, A&A, 4, 234

Gathier, R., Pottasch, S. R., & Pel, J. W. 1986, A&A, 157, 171

Giammanco, C., Sale, S. E., & Corradi, R. L. M., et al. 2011, A&A, 525, A58

Gray, R. O., & Corbally, C. J. 2009, Stellar Spectral Classification (Princeton: Princeton Univ. Press)

Harris, H. C., Dahn, C. C., Monet, D. G., & Pier, J. R. 1997, ed. H. J. Habing, & H. J. G. L. M. Lamers, in IAU Symp. 180, Planetary Nebulae (Dordrecht: Kluwer Academic), 40

Harris, H. C., Dahn, C. C., & Canzian, B., et al. 2007, AJ, 133, 631

Kaler, J. B. 1983, ApJ, 271, 188

———. 1985, ARA&A, 23, 89

Kaler, J. B., & Feibelman, W. A. 1985, ApJ, 297, 724

Kaler, J. B., Shaw, R. A., & Kwitter, K. B. 1990, ApJ, 359, 392

Kiss, L. L., Szabó, G. M., Balog, Z., Parker, Q. A., & Frew, D. J. 2008, MNRAS, 391, 399

Kron, G. E. 1978, AJ, 83, 1195

Landolt, A. U. 1983, AJ, 88, 439

———. 1992, AJ, 104, 340

Lutz, J. H. 1973, ApJ, 181, 135

———. 1989, in IAU Symp. 131, Planetary Nebulae, ed. S. Torres-Peimbert (Cambridge: Cambridge Univ. Press), 65

Maciel, W. J. 1984, A&AS, 55, 253

Majaess, D. J., Turner, D. G., & Lane, D. J. 2007, PASP, 119, 1349

Majaess, D. J., Turner, D. G., Lane, D. J., & Moncrieff, K. E. 2008, J. AAVSO, 36, 90

Meynet, G., Mermilliod, J.-C., & Maeder, A. 1993, A&AS, 98, 477

Milne, D. K., & Aller, L. H. 1975, A&A, 38, 183

Moffat, A. F. J., & Vogt, N. 1977, PASP, 89, 323

Neckel, Th., & Klare, G. 1980, A&AS, 42, 251

Osterbrock, D. E., & Ferland, G. J. 2006, Astrophysics of Gaseous Nebulae and Active Galactic Nuclei (2nd ed.; Sausolito: University Science Books

Parthasarathy, M. 1993, ApJ, 414, L109

Perek, L., & Kohoutek, L. 1967, Catalogue of Galactic Planetary Nebulae (Prague: Academia)

Phillips, J. P. 2004, MNRAS, 353, 589

Phillips, J. P., Cuesta, L., & Kemp, S. N. 2005, MNRAS, 357, 548

Pier, J. R., Harris, H. C., Dahn, C. C., & Monet, D.G. 1993, in IAU Symp. 155, Planetary Nebulae, ed. R. Weinberger & A. Acker (Dordrecht: Kluwer Academic), 175

Pollacco, D. L., & Ramsay, G. 1992, MNRAS, 254, 228

Pottasch, S. R., & Acker, A. 1998, A&A, 329, L5

Purgathofer, A., & Perinotto, M. 1981, A&A, 101, 247

Racine, R., & Harris, W. E. 1975, ApJ, 196, 413

Sale, S. E., Drew, J. E., & Unruh, Y. C., et al. 2009, MNRAS, 392, 407

Schneider, S. E., Terzian, Y., Purgathofer, A., & Perinotto, M. 1983, ApJS, 52, 399

Shklovsky, I. S. 1956, AZh, 33, 222

Soker, N. 1997, ApJS, 112, 487

Terzian, Y. 1997, in IAU Symp. 180, Planetary Nebulae, ed. H. J. Habing, & H. J. G. L. M. Lamers (Dordrecht: Kluwer Academic), 29

Turner, D. G. 1976a, AJ, 81, 97

———. 1976b, AJ, 81, 1125

———. 1979, PASP, 91, 642

———. 1980, ApJ, 240, 137

———. 1983, AJ, 86, 650

———. 1992, AJ, 104, 1865

———. 1994, Rev. Mex. AA, 29, 163

———. 2003, in The Garrison Festschrift, ed. R. O. Gray, C. J. Corbally, & A. G. D. Philip (Schenectady: L. Davis Press), 101

———. 2011, Rev. Mex. AA, 47, 127

Turner, D. G., & Drilling, J. S. 1984, PASP, 96, 292

Turner, D. G., Lyons, R. W., & Bolton, C. T. 1986, Observatory, 106, 13

Turner, D.G., MacLellan, R. F., Henden, A. A., & Berdnikov, L. N. 2011, Rev. Mex. AA, 47, 345

VandenBerg, D. A., Bergbusch, P. A., & Dowler, P. D. 2006, ApJS, 162, 375

Weidemann, V. 2000, A&A, 363, 647

Zhang, C. Y. 1995, ApJS, 98, 659

Ziznovsky, J. 1975, Bull. Astron. Inst. Czechoslovakia, 26, 248